Generation of Metal Nanoparticles from Silver and Copper Objects: Nanoparticle Dynamics on Surfaces and Potential Sources of Nanoparticles in the Environment

Richard D. Glover,[†] John M. Miller,[‡] and James E. Hutchison[†,‡,*]

[†]Department of Chemistry and Materials Science Institute, 1253 University of Oregon, Eugene, Oregon 97403, United States, and [‡]Dune Sciences, Inc., 1900 Millrace Drive, Eugene, Oregon 97403, United States

ABSTRACT The use of silver nanoparticles (AgNPs) in antimicrobial applications, including a wide range of consumer goods and apparel, has attracted attention because of the unknown health and environmental risks associated with these emerging materials. Of particular concern is whether there are new risks that are a direct consequence of their nanoscale size. Identifying those risks associated with nanoscale structure has been difficult due to the fundamental challenge of detecting and monitoring nanoparticles in products or the environment. Here, we introduce a new strategy to directly monitor nanoparticles and their transformations under a variety of environmental conditions. These studies reveal unprecedented dynamic behavior of AgNPs on surfaces. Most notably, under ambient conditions at relative humidities greater than 50%, new silver nanoparticles form in the vicinity of the parent particles. This humidity-dependent formation of new particles was broadly observed for a variety of AgNPs and substrate surface coatings. We hypothesize that nanoparticle production occurs through a process involving three stages: (i) oxidation and dissolution of silver from the surface of the particle, (ii) diffusion of silver ion across the surface in an adsorbed water layer, and (iii) formation of new, smaller particles by chemical and/or photoreduction. Guided by these findings, we investigated non-nanoscale sources of silver such as wire, jewelry, and eating utensils that are placed in contact with surfaces and found that they also formed new nanoparticles. Copper objects display similar reactivity, suggesting that this phenomenon may be more general. These findings challenge conventional thinking about nanoparticle reactivity and imply that the production of new nanoparticles is an intrinsic property of the material that is not strongly size dependent. The discovery that AgNPs and CuNPs are generated spontaneously from manmade objects implies that humans have long been in direct contact with these nanomaterials and that macroscale objects represent a potential source of incidental nanoparticles in the environment.

KEYWORDS: silver nanoparticles · nanosilver · copper nanoparticles · nanomaterial characterization · nanoparticle dynamics · nanoEHS

The proliferation of engineered nanoscale materials in consumer products has raised scientific and public concerns about the potential impacts of those materials on human and environmental health.[1] Particular focus has been placed on whether there are new risks or reactivities that result from the nanoscale size of these materials. Silver nanoparticles (AgNPs) are of particular interest because of their rapidly growing use in antimicrobial applications[2−4] and the known toxicity of silver cation.[5] The key questions regarding AgNPs parallel those for nanomaterials in general: Are nanoparticles released from products?[6−8] What is the fate of those nanoparticles? Are there hazards that are specific to the nanoscale form (including size and surface chemistry)?[1,9,10] What are the implications for Environmental Health Safety (EHS) and regulation?[1]

Answers to these questions have remained elusive, in part, because it is challenging to detect and identify nanomaterials in the environment and even more difficult to monitor the transformation products that result from nanoparticle weathering.[11−13] As a result, much of the currently accepted understanding of the reactivity and fate of nanoparticles has been derived from indirect analysis using solution studies or other model systems from which one can only infer the fate of particles.[6,14,15] For AgNPs, these indirect analyses focus on quantification of silver retained or released, but do not provide the speciation. Several studies have determined that AgNPs in solution release ionic silver (Ag^+) and that the rate of Ag^+ release is influenced by particle size, particle functionalization, and the local environment.[9,10] To date, however, no studies have been reported where the nanoparticles can be directly monitored over time to determine their behavior. As a consequence, one cannot accurately predict AgNP behavior or their potential hazards when they are deposited on or embedded

* Address correspondence to hutch@uoregon.edu.

Received for review August 16, 2011 and accepted October 10, 2011.

Published online October 10, 2011
10.1021/nn2031319

in surfaces, as they are in the majority of the antimicrobial applications.

In this paper, we introduce a versatile strategy for the direct visualization of nanoparticle transformations on solid surfaces. This integrated strategy comprises (i) the capture and immobilization of nanoparticles on a functionalized characterization substrate, (ii) the *in situ* weathering of these particles, and (iii) the multitechnique characterization of identical particles over time. The use of silicon-based TEM grid substrates with thermal oxide membrane windows ensures the compatibility and durability of the substrate during relevant environmental exposures. The grids are chemically functionalized to capture and tether them on the grid surface with a high dispersion.[16] Once they have been securely anchored to the grid, the nanoparticles can be exposed to a wide range of controlled environmental conditions. The nanoparticle structure and composition can be monitored over time by methods such as TEM, UHV surface analysis, and scanning probe microscopies. By indexing individual particles to the grid, the same particles can be reanalyzed after exposure to monitor temporal changes. Here we describe a practical application of this strategy to the case of AgNPs on surfaces. This platform permitted the direct observation of the formation of small nanoparticles in the vicinity of the tethered nanoparticles and provide insight into the material dynamics behind this reactivity. The approach was extended to capture and image nanoparticles generated from macroscale silver and copper objects (*e.g.*, cutlery and jewelry).

RESULTS AND DISCUSSION

To assess how environmental conditions affect the structure and stability of AgNPs, samples were prepared for analysis by immobilizing 10 and 75 nm PVP and citrate-stabilized and 20 nm polysorbate-20-stabilized AgNPs on positively charged, amine functionalized SMART Grids through electrostatic interactions (Figure 1A). For all data shown, unless noted, 75 nm PVP-stabilized particles were used. The resulting specimens showed remarkably uniform distributions of well-isolated particles anchored across the grid surface (Figure 1B) that are ideally suited for indexed imaging. The goal of this work was to directly visualize time-resolved evolution and reactivity of AgNPs deposited on surfaces when exposed to light, humidity, and aqueous solutions (water, salt, bleach, *etc.*).

Formation of New Nanoparticles from AgNPs Bound to Surfaces. A key finding from our survey of the effects of environmental conditions on tethered AgNPs is that they transform extensively on the grid surface even in the absence of a solution phase. Specifically, upon exposure to ambient laboratory conditions, new smaller particles were observed on the surface near the nanoparticles that had been originally assembled on the grid (Figure 1C).

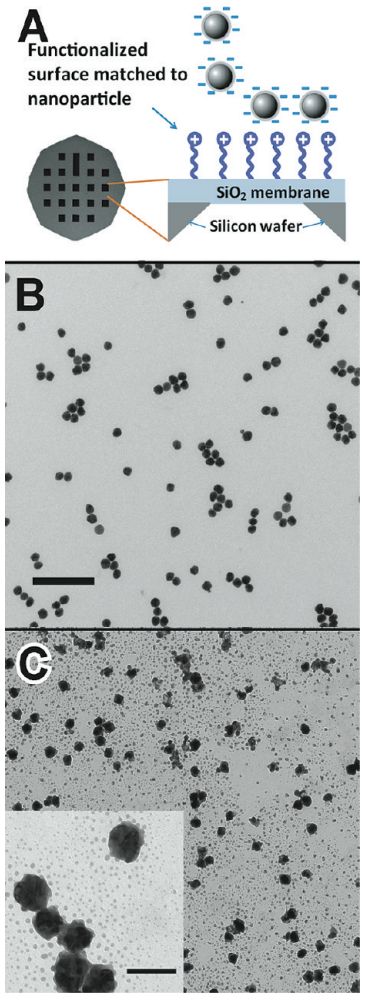

Figure 1. Direct visualization of morphological changes in surface-bound AgNPs under ambient conditions. (A) Strategy for tethering NPs on positively charged SiO_2 grids; 75 nm PVP-stabilized AgNPs were used as the starting point for each of the experiments shown in panels B and C. (B) TEM image showing freshly tethered 75 nm PVP-stabilized AgNPs with uniform distribution across the grid. (C) TEM image showing the growth of small particles in the vicinity of the parent particles after storage in air under ambient laboratory conditions for 4 weeks. Inset shows a zoomed-in image of new nanoparticles formed in the vicinity of the parent particles. The scale bar for panels B and C are 500 and 100 nm for the inset.

These smaller particles were not isolated to selected areas but were prevalent across every sample measured. The discovery of small particles on the grid was surprising because freshly deposited 75 nm samples showed no evidence of smaller nanoparticles, and AgNP solutions themselves are stable in dark, cool environments for several months. Yet, particles deposited on the surface of the grids began to show transformations in size, shape, and particle population within a few hours. This finding highlighted the need to directly observe the behavior of nanomaterials on surfaces.

An initial study was conducted to determine the influence of humidity and light on the formation of these new nanoparticles. Figure 2 shows a series of

TEM micrographs for the samples exposed to controlled humidity conditions for 3 weeks. The sample stored at 0% relative humidity (RH) remains unchanged over this period, whereas those stored under humid conditions show dramatic morphological changes. New small particles were abundant in the vicinity of particles stored at 100% RH suggesting that humidity plays an important role in their formation. Samples stored at 50% RH showed less pronounced changes that could be characterized as nanoscale protrusions from the parent particles. In these experiments, light exposure had a significant influence on the extent of particle degradation and formation (Supporting Information Figure S1). Therefore, subsequent experiments were conducted in the dark with minimal exposure to light during transfer in and out of the TEM to provide more controlled conditions for monitoring nanoparticle degradation. Given that water adsorption to surfaces is dependent on RH,[17] these results suggest that the structure of the adsorbed water layer may influence the transformations of the parent AgNPs.

To gain insight into the temporal changes of individual nanoparticles and to better understand this dynamic behavior, an indexing protocol was developed to characterize the same nanoparticles over time. Figure 3 shows a series of images for the same population of five 75 nm PVP-stabilized AgNPs exposed to 100% RH over 5 weeks. After the first week, new particles were observed in the immediate vicinity of the five larger particles. After 3 weeks and 5 weeks, additional small particles were observed surrounding the parent particles. Notably, the particles formed during the previous time point remain fixed in space, whereas the newer particles form farther away from the parent particles.

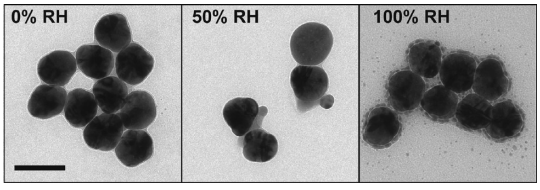

Figure 2. Humidity-induced morphological changes to AgNPs deposited on amine-functionalized grids. TEM images of the particles stored for 3 weeks under different humidity conditions (%RH) show morphological changes and the appearance of small particles under humid conditions. The scale bar is 100 nm for all three panels.

Characterization of New Nanoparticle Formation. The formation of smaller nanoparticles under humid conditions raises several questions: (i) Is the electron beam responsible for nanoparticle formation? (ii) What is the composition of the new nanoparticles? and (iii) Does the grid surface chemistry facilitate their formation? A series of control experiments was conducted to examine each of these questions. First, atomic force microscopy (AFM) was used to examine these transformations without exposure to the TEM's electron beam. The AFM images (Supporting Information Figure S2) collected for samples assembled on atomically flat mica substrates show that new particles are formed in the vicinity of the original particles after environmental exposure. These results suggest that the presence of these particles is not simply induced by the electron beam in the TEM.

Next, energy dispersive X-ray spectroscopy (EDS), X-ray photoelectron spectroscopy (XPS), and selected area diffraction (SAD) were used to determine the composition of newly formed particles on the substrate (Figure 4A). Highly degraded 10 nm PVP-stabilized AgNPs were used for EDS and SAD analysis due to the higher surface coverage of these samples. EDS spectra (Figure 4C,D) showed only Si, O, and Ag (Si and O are a result of the SiO_2 grid). There is no evidence of sulfur (2.3 eV) or chlorine (2.6 eV) present that would suggest the formation of Ag_2S or AgCl. The binding energies of the silver peaks in the XPS provides a means of distinguishing Ag° from Ag_2O. The position of the Ag $3d_{5/2}$ peak (368.6 eV) in the XPS spectrum of the silver nanoparticles in Supporting Information Figure S3 is consistent with Ag° and is found at higher binding energy than typically found for Ag_2O.[18]

To confirm the conclusions drawn from EDS and XPS, SAD was performed over an area containing new nanoparticles. The diffraction pattern shown in Figure 4B confirms that the new particles are comprised primarily of fcc Ag.[19] Taken together, EDX, XPS, and SAD strongly suggest that the nanoparticles are composed primarily of Ag°.

To investigate whether the grid surface chemistry influences nanoparticle formation, AgNPs were

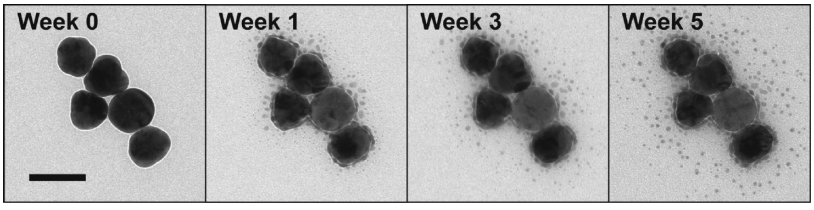

Figure 3. Ⓦ Formation of small nanoparticles in the vicinity of 75 nm AgNPs at 100% RH over five weeks. TEM images taken during the exposure period show increasing numbers of small nanoparticles (0, 262, 290, and 312, respectively) throughout this time frame. The details of the changes to these structures are most easily visualized in a movie composed of the sequential images (Movie 1). The scale bar is 100 nm for all panels.

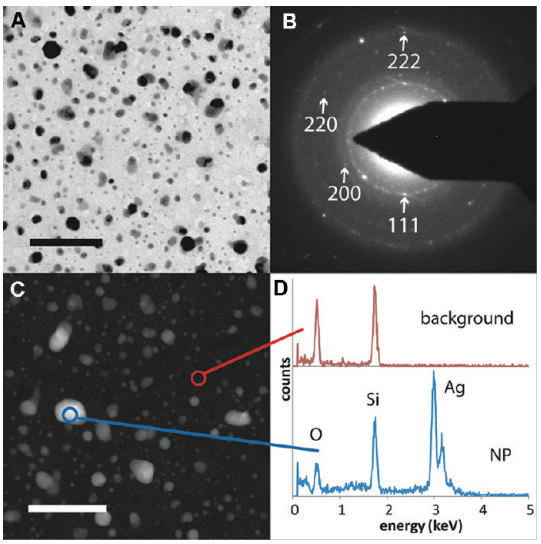

Figure 4. Characterization of the chemical composition of transformed 10 nm PVP stabilized AgNPs. (A) Bright field TEM image of transformed particles. (B) Selected area diffraction corresponding to the field of view in panel A. The measured rings correspond to the (111), (200), (220), and (222) faces of fcc Ag. (C) HAADF-STEM image of the transformed particles. The areas identified by circles represent the sample area examined by EDS. (D) EDS spectra for the areas indicated in panel C. The top spectrum (red) corresponds to substrate/background and the bottom spectrum (blue) corresponds to AgNPs. All scale bars shown are 100 nm.

deposited on nonfunctionalized SiO_2 TEM grids and similar transformations were observed (Supporting Information Figure S4). These observations, taken together with the results obtained on the mica surfaces during the AFM investigations, rule out the possibility that the positively charged hydrophilic surface catalyzes the nanoparticle transformations. Although there may be subtle changes in the rate and extent of nanoparticle formation on different surfaces, the formation of new particles appears to be a general phenomenon that is not significantly impacted by the nature of the substrate surface.

On the basis of the results described here, we propose a three-stage pathway for new nanoparticle formation (Figure 5). In the first stage, the surface of the silver nanoparticles becomes oxidized in the presence of oxygen and water, generating silver ions that dissolve in the humidity-dependent adsorbed water layer.[17] The release of silver ions from silver nanoparticles as an oxidation product under aerobic, aqueous conditions has been well-established and is not expected to be significantly impeded by the weak passivating ligands used in these experiments.[9,10,20] However, the small volume of the surface water layer means that it will rapidly become saturated with silver cations (see calculations in Supporting Information Table S1).

In the second stage, dissolved silver ions diffuse away from the parent particles in the absorbed water layer as a result of the strong concentration gradients

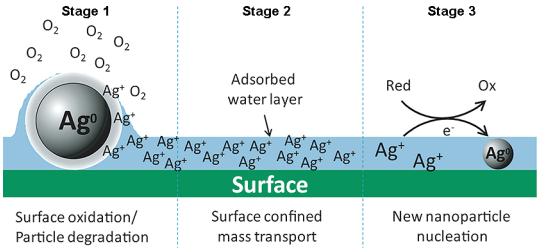

Figure 5. Proposed pathway for new particle formation away from parent nanoparticles. The pathway is broken into three stages in the figure. Stage 1 involves surface oxidation with ambient oxygen and adsorbed water. In stage 2, ionized silver diffuses away from the parent particle in the adsorbed water layer driven by the concentration gradient. During stage 3 new particles nucleate *via* chemical and/or photochemical reduction of silver ion on the surface.

around the parent particles. As shown in Figure 3 and in Movie 1, once formed, the new nanoparticles do not move. Additional particles are formed farther away from the parent particles over time, suggesting that the mobile species are silver ions, not the particles themselves. The mobility of silver ions in an adsorbed water layer on surfaces has been reported in systems with electrochemical gradients.[21,22] For relatively polar surfaces such as those employed here, at 100% humidity, the water layer is thin (less than 3 nm), yet thick enough that a liquid-like layer is present that should facilitate transport of the ions away from the parent NP (as seen in our experiments).[17] However, because the layer is so thin, the diffusion of ions will be slowed by interactions of the water layer with the surface.[23] These effects on ion diffusion will likely influence the location at which new particles are formed. At lower relative humidities, a thinner hydrogen bonded (ice-like) layer is present that has been suggested to be less effective for ion transport.[17] This notion is consistent with our findings at 50% RH in which the particles show morphological changes, but no significant new particle formation.

In the third stage, new smaller Ag° nanoparticles are produced through reduction of the silver ions on the surface. AgNPs are readily nucleated by a variety of mild reductants[24,25] and/or through photoreduction.[26−28] In this case, it is likely that reduction occurs through multiple pathways. Although the humidity experiments were conducted in the dark, brief exposure to stray light during sample transfer to the microscope was difficult to prevent and likely contributed to photoreduction. In addition, several of the chemical coatings or stabilizers (PVP, citrate, and aminoalkylsilanes) are known to reduce silver ion to produce AgNPs.[24,29,30] Thus, while the data clearly show the formation of new nanoparticles, given the ease of reduction, the number of potential chemical reductants, light sensitivity of silver ions and the subsequent exposure to the electron beam, it was not possible to isolate a single agent or exposure responsible for reduction.

The production of small particles by the transfer of ions from large particles might be thought to increase the free energy of the system due to increased surface energy of the small particles; however, there are several factors that may contribute to the stability of these new particles. First, the smaller particles may be stabilized by specific interactions with the surface that develop during their nucleation and growth. Next, the combination of slow diffusion, lower temperatures, and widely spaced parent particles favors the formation of the smaller, kinetically stabilized particles that we observe. Finally, it has been recently reported that smaller nanoparticles are more stable when the concentration of surrounding large particles is lower,[31] as is the case here. Although additional investigations will be required to explore the details of the dynamics of these nanoparticles on surfaces, it is clear that the dynamics are significantly different than those in the solution phase.

The three-stage process described here predicts that all AgNPs passivated with a weakly bound ligand shell should generate small particles on surfaces exposed to humidity. Our results support that prediction because we observed similar transformations with AgNPs of different sizes and stabilizers (10 nm PVP, 75 nm PVP, 75 nm citrate, and 20 nm polysorbate-20) (Supporting Information Figure S5). One important question that remains is whether this phenomenon is restricted to nanoscale materials.

Formation of New Nanoparticles from Silver Wire and Other Objects. To determine whether the formation of new nanoparticles is a more general phenomenon, we investigated several common silver objects to see whether they might also generate small nanoparticles when in contact with a surface. Our rationale was that if oxidation of the surface and dissolution of silver ions (analogous to stage 1 in Figure 5) occurs for macroscale objects[20] in contact with surfaces, then stages 2 and 3 should follow to produce new small nanoparticles in the vicinity of these objects. To probe this question, a silver wire and a sterling silver earring were placed on grids (Figure 6 panels A and C), exposed to humid conditions, and the grids were examined by TEM. The images in Figure 6B,D show that in both cases a heterogeneous population of nanoparticles was deposited in the vicinity where each object had contacted the grid. These results are unexpected based upon the extensive investigations of nanosilver that have been reported. Further, they suggest that silver-containing consumer products and other objects that are frequently in contact with human skin readily form AgNPs.

To further probe the role of water in these transformations, a small droplet of water was placed at the interface between the object and the substrate to determine whether nanoparticle formation is accelerated in the presence of bulk water. A silver-plated

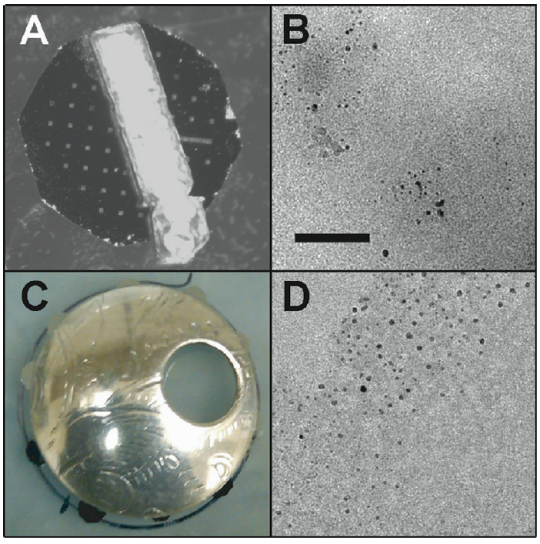

Figure 6. Generation of AgNPs from silver wire and a sterling silver earring. (A) An optical image showing a silver wire in direct contact with an amine-functionalized grid. (B) A TEM image revealing that nanoparticles are generated during contact with the wire over 3 weeks at 100% RH. (C) An optical image of a sterling silver earring placed in direct contact with several amine-functionalized grids. (D) A TEM image showing the nanoparticles that were generated during contact with the earring over 3 weeks at 100% RH. In these experiments samples were exposed to intermittent light throughout the experiment. The scale bar shown is 50 nm for panels B and D.

spoon and fork (Figure 7A) were each placed onto a 1 μL droplet of water and the water was allowed to evaporate on the grid. Remarkably, in the time it took for the droplet to dry (<10 min) large numbers of small particles were produced (Figure 7B). We characterized the nanoparticles by EDS to determine their composition. Figure 7 panels B and C show a HAADF-STEM image of the nanoparticles formed from the object and the corresponding EDS spectrum for the area shown in Figure 7C confirms the bulk of the material is silver (indicated by the peaks at 2.7, 3.0, and 3.2 keV). There are trace amounts of sulfur (2.3 keV), chlorine (2.8 keV), and copper (0.9 keV) that are common silver oxidants and/or are consistent with tarnished silver.[32] The rapid generation of nanoparticles under these conditions is consistent with the model shown in Figure 5 because the larger volume of water has the potential to dissolve more silver that would then be concentrated to saturation during the evaporation of the droplet. This might also explain why the nanoparticles are larger and more heterogeneous than in the humidity experiments. These results demonstrate that nanoparticles can be formed from any silver object in contact with water alone.

Considering our findings with silver, we wondered whether other metals that are easily oxidized and reduced under environmental conditions (*e.g.,* copper) might exhibit similar behavior.[21] Copper wire (Figure 8) was investigated in the same manner as for the silver

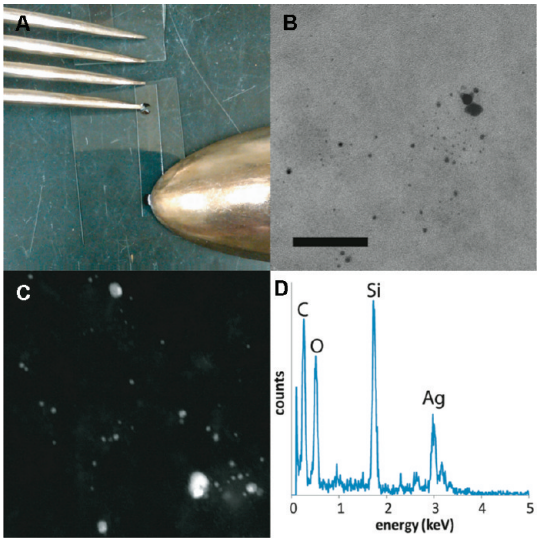

Figure 7. Generation of AgNPs from common silver objects. (A) An optical image of a sterling silver knife and fork in contact with the grid surfaces. (B) A TEM image of particles produced upon introduction and evaporation of a 1 μL droplet of water. (C) A HAADF-STEM image of particles produced upon drying as in panel B. (D) EDS spectrum of the generated nanoparticles that confirms their composition is silver. The additional elements (oxygen and silicon) arise from the SiO_2 substrate. The scale bar shown is 50 nm for both panels B and C.

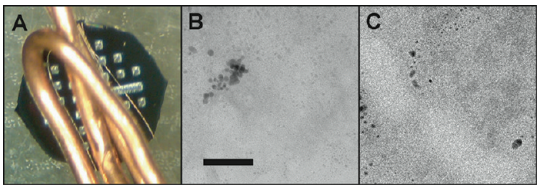

Figure 8. Generation of CuNPs from copper wire. (A) Optical image of copper wire in contact with the surface of a grid. (B) A TEM image showing CuNPs produced when the wire was left on the grid for 7 days at 100% RH. (C) A TEM image showing CuNPs formed when a 1 μL droplet of water was introduced and allowed to dry. Scale bar shown is 50 nm for panels B and C.

objects. Nanoparticles were produced at 100% RH and in the droplet experiment just as in the case of silver. EDS confirmed that the composition of the particles was copper (Supporting Information Figure S6). These results provide additional evidence that the three-stage process for nanoparticle formation shown in Figure 5 may be a general phenomenon that is a potential source of metal nanoparticles in the environment.

CONCLUSIONS

The strategy employed in this study represents a new approach in which the fate of nanomaterials can be directly measured after exposure to a range of environmental stimuli. We find that all silver, whether nano- or macro-scale, generates AgNPs when exposed to humid air or water. We characterized production of the nanoparticles as occurring in three distinct stages: (i) ionization of Ag° and dissolution of Ag^{+}, (ii) diffusion of silver ions away from metal of origin in the adsorbed water layer, and (iii) reduction of Ag^{+} under ambient conditions. Studies with copper wire also produce nanoparticles, suggesting that this process may be general for metals that can be readily oxidized and reduced under environmental conditions. These findings provide significant new insight into the dynamics of nanoparticles bound to surfaces. In the present study, silver ions are released into, confined by, and reduced within the adsorbed water layer, leading to profoundly different reactivity than in solution.

The dynamic nature of surface-bound nanoparticles has profound implications for our understanding of metal speciation in the environment, the dynamics of nanoparticle reactivity, and our approaches to nanomaterial health and safety and the regulation of these materials. Our findings suggest that differentiating material hazards by size can be misleading. The fact that nanoparticles are spontaneously produced suggests that Ag and Cu NPs have been present as incidental nanomaterials and in contact with humans for several thousand years. The generation of nanoparticles may be a general phenomenon for materials oxidized and reduced under common environmental conditions. EHS and regulatory policy should recognize the presence of background levels of nanoparticles and their dynamic behavior in the environment. On a broader scale, these findings highlight the need for new characterization strategies to assess nanomaterial transformations under environmentally relevant conditions. Finally, the results beg the question of what other incidental nanomaterials might exist in nature that we have not developed the tools to detect.

METHODS

Silver Nanoparticles. Silver nanoparticles used in this study were purchased from commercial suppliers. The 75 nm PVP-stabilized AgNPs used in this study were purchased from Nanocomposix. As received, these particles have a concentration of 1 mg/mL in water. Additional materials that were evaluated include 10 and 75 nm citrate-stabilized AgNPs (Nanocomposix) and 20 nm polysorbate-20-stabilized AgNPs (Dune Sciences). Sample vials were stored in the dark at 4 °C when not in use. All nanoparticles were sonicated for 30 s to ensure complete dispersion of the particles prior to deposition.

Substrates. SMART Grids TEM substrates were provided by Dune Sciences and used as received. The grids are 3 mm silicon disks with 50 μm $\times$ 50 μm electron-transparent SiO_2 windows that are silanized with different functional groups to promote the capture of different types of materials.[16] Amine-functionalized, positively charged grids were selected to enhance the affinity for the AgNPs through electrostatic interactions. We also

conducted experiments with nonfunctionalized grids to rule out any substrate effects related to the surface chemistry on the grid. Mica substrates were purchased from Ted Pella. Fresh mica surfaces were generated by removing the top layers using adhesive tape. The mica surfaces were silanized by soaking for 1 h in a 0.017 mM aqueous 1-(3-aminopropyl)silatrane solution.[33]

Capturing Nanoparticles on the Grids and Mica Surfaces. To capture nanoparticles, the amine-functionalized grids were floated for 5 min on individual 5 μL droplets of AgNP solution (as received) that were deposited on parafilm. Each grid was removed from the droplet and lightly contacted on the edge with filter paper to wick away excess solution. Next, the grid was floated on a droplet of nanopure water for five minutes to rinse away any unbound materials. Finally, the grids were removed from the droplet and dried in air. Once dried, the grids were stored in a dark chamber at 0% RH for up to 1 day. For the nonfunctionalized TEM grids, the rinse step was omitted because the particles are not captured and bound by the grid surface and are thus easily displaced.

Controlled Exposure to Humid Conditions. Samples were stored in humidity-controlled environments for up to 5 weeks using the following conditions: 0% RH, sample stored in desiccation chamber; 50% RH, sample stored in humidity controlled room; and 100% RH, sample stored in chamber containing a reservoir of liquid water. All samples were stored in the dark to control degradation/renucleation from ambient light; however, incidental exposure to light occurred when removing grids from chambers and preparing samples for TEM analysis.

Transmission Electron Microscopy (TEM) Imaging. Bright field TEM analysis was performed using FEI Tecnai Spirit TEM operated at 120 kV or FEI Titan TEM operated at 300 kV. High angular annular dark field scanning transmission electron microscopy (HAADF-STEM) images were taken using the FEI Titan. Energy dispersive X-ray spectroscopy (EDS) was used for chemical analysis in HAADF-STEM mode.

To image the same location on a grid during extended humidity exposures, the location of particles was denoted relative to the indexing window and the grid was oriented in the same position each time it was imaged. Using a window corner as a guide the same particles were identified and images were taken at identical magnification. Images were aligned using Linear Stack Alignment with SIFT in Image J so that changes between images could be compared more easily. To serve as a visual aid, an animated video was prepared from the registered images taken over the course of treatment (Movie 1).[34,35]

Atomic Force Microscopy (AFM). AFM was used in noncontact tapping mode on a Veeco Nanoscope IIIA with Nanosensor POINTPROBE-PLUS Silicon-SPM Sensor tips, resonant frequency range of 204−497 kHz. The scan area was 800 nm_2, scan rate was 0.5 Hz, with 512 × 512 samples over the area. Images were taken in phase contrast mode.

X-ray Photoelectron Spectroscopy (XPS). XPS spectra were taken at 20 eV pass energy on a ThermoFisher ESCALab 250 with a monochromated Al K-alpha, using a 400 μm spot size. Each spectrum was corrected to aliphatic carbon at 284.8 eV. Peak fitting of the Ag $3d_{5/2}$ was done using ThermoFisher Avantage software.

Acknowledgment. We thank E. W. Elliott III for developing the image registration protocol and S. Xie and J. Razink at the Center for Advanced Materials Characterization in Oregon (CAMCOR) TEM Facility for assistance with the TEM imaging. This work was supported by the Air Force Research Laboratory (under Agreement No. FA8650-05-1-5041) and the W. M. Keck Foundation. R.D.G. acknowledges support from the National Science Foundation Graduate STEM Fellows in K-12 Education Program under Grant No. DGE-0742540. The CAMCOR TEM facility is supported with grants from the W. M. Keck Foundation, the M. J. Murdock Charitable Trust, the Oregon Nanoscience and Microtechnologies Institute, and the University of Oregon.

Supporting Information Available: AFM images of freshly deposited and aged AgNPs on mica; XPS spectra of freshly deposited and aged AgNPs; TEM images of particles on nonfunctionalized TEM images; a table showing the estimated concentration of silver ion in the adsorbed water layer; TEM and EDS of CuNPs. This material is available free of charge *via* the Internet at http://pubs.acs.org.

Web Enhanced. A movie composed of the indexed images from Figure 3 overlaid to highlight the NP transformations is available in the HTML version of the paper.

REFERENCES AND NOTES

1. Krug, H. F.; Wick, P. Nanotoxicology: An Interdisciplinary Challenge. *Angew. Chem., Int. Ed.* **2011**, *50*, 1260–1278.
2. Nowack, B.; Krug, H. F.; Height, M. 120 Years of Nanosilver History: Implications for Policy Makers. *Environ. Sci. Technol.* **2011**, *45*, 1177–1183.
3. Cioffi, N.; Torsi, L.; Ditaranto, N.; Tantillo, G.; Ghibelli, L.; Sabbatini, L.; Bleve-Zacheo, T.; D'Alessio, M.; Zambonin, P. G.; Traversa, E. Copper Nanoparticle/Polymer Composites with Antifungal and Bacteriostatic Properties. *Chem. Mater.* **2005**, *17*, 5255–5262.
4. Rai, M.; Yadav, A.; Gade, A. Silver Nanoparticles as a New Generation of Antimicrobials. *Biotechnol. Adv.* **2009**, *27*, 76–83.
5. Casarett, L. J.; Doull, J.; Klaassen, C. D. *Casarett and Doull's Toxicology: The Basic Science of Poisons*; McGraw-Hill: New York, 2008.
6. Kittler, S.; Greulich, C.; Diendorf, J.; Köller, M.; Epple, M. Toxicity of Silver Nanoparticles Increases during Storage Because of Slow Dissolution under Release of Silver Ions. *Chem. Mater.* **2010**, *22*, 4548–4554.
7. Kulthong, K.; Srisung, S.; Boonpavanitchakul, K.; Kangwansupamonkon, W.; Maniratanachote, R. Determination of Silver Nanoparticle Release from Antibacterial Fabrics into Artificial Sweat. *Part. Fibre Toxicol.* **2010**, *7*, 1–9.
8. Benn, T. M.; Westerhoff, P. Nanoparticle Silver Released into Water from Commercially Available Sock Fabrics. *Environ. Sci. Technol.* **2008**, *42*, 4133–4139.
9. Liu, J.; Hurt, R. H. Ion Release Kinetics and Particle Persistence in Aqueous Nano-Silver Colloids. *Environ. Sci. Technol.* **2010**, *44*, 2169–2175.
10. Liu, J.; Sonshine, D. A.; Shervani, S.; Hurt, R. H. Controlled Release of Biologically Active Silver from Nanosilver Surfaces. *ACS Nano* **2010**, *4*, 6903–6913.
11. Maccuspie, R. I.; Rogers, K.; Patra, M.; Suo, Z.; Allen, A. J.; Martin, M. N.; Hackley, V. A. Challenges for Physical Characterization of Silver Nanoparticles Under Pristine and Environmentally Relevant Conditions. *J. Environ. Monit.* **2011**, *13*, 1212–1226.
12. Richman, E. K.; Hutchison, J. E. The Nanomaterial Characterization Bottleneck. *ACS Nano* **2009**, *3*, 2441–2446.
13. Nowack, B. Nanosilver Revisited Downstream. *Science* **2010**, *330*, 1054–1055.
14. Geranio, L.; Heuberger, M.; Nowack, B. The Behavior of Silver Nanotextiles during Washing. *Environ. Sci. Technol.* **2009**, *43*, 8113–8118.
15. Impellitteri, C. A.; Tolaymat, T. M.; Scheckel, K. G. Speciation of Silver Nanoparticles in Antimicrobial Fabric before and after Exposure to a Hypochlorite/Detergent Solution. *J. Environ. Qual.* **2009**, *38*, 1528–1530.
16. Kearns, G. J.; Foster, E. W.; Hutchison, J. E. Substrates for Direct Imaging of Chemically Functionalized SiO_2 Surfaces by Transmission Electron Microscopy. *Anal. Chem.* **2006**, *78*, 298–303.
17. Asay, D. B.; Kim, S. H. Evolution of the Adsorbed Water Layer Structure on Silicon Oxide at Room Temperature. *J. Phys. Chem. C.* **2005**, *109*, 16760–16763.
18. Shin, H. S.; Choi, H. C.; Jung, Y.; Kim, S. B.; Song, H. J.; Shin, H. J. Chemical and Size Effects of Nanocomposites of Silver and Polyvinyl Pyrrolidone Determined by X-ray Photoemission Spectroscopy. *Chem. Phys. Lett.* **2004**, *383*, 418–422.
19. Chen, R.; Nuhfer, N.; Moussa, L.; Morris, H. Silver Sulfide Nanoparticle Assembly Obtained by Reacting an Assembled Silver Nanoparticle Template with Hydrogen Sulfide Gas. *Nanotechnol.* **2008**, *19*, 455604.

20. Graedel, T. E. Corrosion Mechanisms for Silver Exposed to the Atmosphere. *J. Electrochem. Soc.* **1992**, *139*, 1963.
21. Conway, B. E.; Bockris, J. O. The Mechanism of Electrolytic Metal Deposition. *Proc. R. Soc. A* **1958**, *248*, 394–403.
22. Yang, S.; Wu, J.; Christou, A. Initial Stage of Silver Electrochemical Migration Degradation. *Microelectron. Reliab.* **2006**, *46*, 1915–1921.
23. Kerisit, S.; Liu, C. Molecular Simulations of Water and Ion Diffusion in Nanosized Mineral Fractures. *Environ. Sci. Technol.* **2009**, *43*, 777–782.
24. Akaighe, N.; Maccuspie, R. I.; Navarro, D. A.; Aga, D. S.; Banerjee, S.; Sohn, M.; Sharma, V. K. Humic Acid-Induced Silver Nanoparticle Formation under Environmentally Relevant Conditions. *Environ. Sci. Technol.* **2011**, *45*, 3895–901.
25. Tolaymat, T. M.; El Badawy, A. M.; Genaidy, A.; Scheckel, K.; Luxton, T. P.; Suidan, M. An Evidence Based Environmental Perspective of Manufactured Silver Nanoparticle in Synthesis and Applications. *Sci. Total Environ.* **2010**, *408*, 999–1006.
26. Pukies, J.; Roebke, W.; Henglein, A. Pulsradiolytische Untersuchung Einiger Elementarprozesse der Silberreduktion (Pulse Radiolysis Study of Some Elementary Processes of Silver Reduction). *Ber. Bunsen. Phys. Chem.* **1968**, *72*, 842–847.
27. Tausch-Treml, R.; Henglein, A.; Lilie, J. Reactivity of Silver Atoms in Aqueous Solution II. A Pulse Radiolysis Study. *Ber. Bunsen. Phys. Chem.* **1978**, *82*, 1335–1343.
28. Sudeep, P. K.; Kamat, P. V. Photosensitized Growth of Silver Nanoparticles under Visible Light Irradiation: A Mechanistic Investigation. *Chem. Mater.* **2005**, *17*, 5404–5410.
29. Huang, H. H.; Ni, X. P.; Loy, G. L.; Chew, C. H.; Tan, K. L.; Loh, F. C.; Deng, J. F.; Xu, G. Q. Photochemical Formation of Silver Nanoparticles in Poly(*N*-vinylpyrrolidone). *Langmuir* **1996**, *12*, 909–912.
30. Choi, Y.; Huh, U.; Luo, T. M. Spontaneous Formation of Silver Nanoparticles in Aminosilica. *J. Sol-Gel Sci. Technol.* **2009**, *51*, 124–132.
31. Gentry, S. T.; Kendra, S. F.; Bezpalko, M. W. Ostwald Ripening in Metallic Nanoparticles: Stochastic Kinetics. *J. Phys. Chem. C.* **2011**, *115*, 12736–12741.
32. Franey, J. P.; Kammlott, G. W.; Graedel, T. E. The Corrosion of Silver by Atmospheric Sulfurous Gases. *Corros. Sci.* **1985**, *25*, 133–143.
33. Shlyakhtenko, L. S.; Gall, A. A.; Filonov, A.; Cerovac, Z.; Lushnikov, A.; Lyubchenko, Y. L. Silatrane-Based Surface Chemistry for Immobilization of DNA, Protein-DNA Complexes, and Other Biological Materials. *Ultramicroscopy* **2003**, *97*, 279–87.
34. Lowe, D. G. Distinctive Image Features from Scale-Invariant Keypoints. *Int. J. Comput. Vision* **2004**, *60*, 91–110.
35. Abràmoff, M. D.; Magalhães, P. J.; Ram, S. J. Image Processing with ImageJ. *Biophoton. Int.* **2004**, *11*, 36–42.